Applied Catalysis B: Environmental 117–118 (2012) 73–80

Contents lists available at SciVerse ScienceDirect

Applied Catalysis B: Environmental

journal homepage: www.elsevier.com/locate/apcatb

Fe–Ti spinel for the selective catalytic reduction of NO with NH_3: Mechanism and structure–activity relationship

Shijian Yang[a,b], Junhua Li[b,*], Chizhong Wang[b], Jinghuan Chen[b], Lei Ma[b], Huazhen Chang[b], Liang Chen[b], Yue peng[b], Naiqiang Yan[a,*]

[a] School of Environmental Science and Engineering, Shanghai Jiao Tong University, Shanghai 200240, PR China
[b] School of Environment, Tsinghua University, Beijing 100084, PR China

ARTICLE INFO

Article history:
Received 5 September 2011
Received in revised form
18 December 2011
Accepted 2 January 2012
Available online 10 January 2012

Keywords:
$(Fe_{3-x}Ti_x)_{1-\delta}O_4$
DRIFTS
Structure–activity relationship
Mechanism
Kinetic analysis

ABSTRACT

A series of non-stoichiometric Fe–Ti spinel $(Fe_{3-x}Ti_x)_{1-\delta}O_4$ were synthesized using a co-precipitation method and then developed as environmental-friendly and low cost catalysts for the selective catalytic reduction (SCR) of NO with NH_3. As Ti was incorporated into γ-Fe_2O_3, the SCR reaction over $(Fe_{3-x}Ti_x)_{1-\delta}O_4$ through the Langmuir–Hinshelwood mechanism was restrained. Therefore, the SCR activity of $(Fe_{3-x}Ti_x)_{1-\delta}O_4$ ($x \neq 0$) was less than that of γ-Fe_2O_3 at 150–250 °C. However, the SCR reaction over $(Fe_{3-x}Ti_x)_{1-\delta}O_4$ through the Eley–Rideal mechanism was promoted due to the incorporation of Ti. The SCR activity of $(Fe_{3-x}Ti_x)_{1-\delta}O_4$ ($x \neq 0$) was mainly related to the oxidative ability of Fe^{3+} cation on the surface, the concentration of NH_3 adsorbed on the surface and the concentration of reducible Fe^{3+} cation on the surface. Although the oxidative ability of Fe^{3+} cation on the surface decreased due to the incorporation of Ti into γ-Fe_2O_3, the concentration of NH_3 adsorbed on the surface and the concentration of reducible Fe^{3+} cation on the surface both increased. As a result, $(Fe_2Ti)_{0.8}O_4$ showed excellent activity, selectivity, and H_2O/SO_2 durability for the SCR reaction at 300–400 °C.

1. Introduction

Nitrogen oxides (NO_x), which are from automobile exhaust gas and flue gas of industrial combustion of fossil fuels, are a major cause for photochemical smog, acid rain and ozone depletion [1]. So far, the most efficient technology for the removal of nitrogen oxides from coal-fired power plants is selective catalytic reduction (SCR) of NO with NH_3. Although V_2O_5–$WO_3(MoO_3)/TiO_2$ has been widely employed as a SCR catalyst to control the emission of NO_x from coal-fired power plants for several decades [2], some problems still exist, such as the relatively narrow temperature window of 300–400 °C, the low N_2 selectivity at high temperature, and the toxicity of vanadium pentoxide to the environment [3]. Therefore, a few researchers have focused on the exploitation of new kinds of SCR catalysts to substitute the conventional vanadium-based catalyst. Recently, it is reported that Fe-based catalysts for example Fe/ZSM-5 [4], Fe^{3+} exchanged TiO_2-pillared clay [5] and iron titanate [6–10] show excellent SCR activity and N_2 selectivity in the relatively high temperature range.

Two Fe^{3+} cations in magnetite (Fe_3O_4) can be substituted by one Ti^{4+} cation and one Fe^{2+} cation to form $Fe_{3-x}Ti_xO_4$. As is well known, nanosized titanomagnetite ($Fe_{3-x}Ti_xO_4$) is extensively distributed in the crust of earth [11,12]. $Fe_{3-x}Ti_xO_4$ can be oxidized to non-stoichiometric Fe–Ti spinel $(Fe_{3-x}Ti_x)_{1-\delta}O_4$ while maintaining the spinel structure [13]. δ is equal to $((1+x)/(9+x))$ if all Fe^{2+} cations in $Fe_{3-x}Ti_xO_4$ are oxidized to Fe^{3+} cations [14]. Our previous research has demonstrated that titanomagnetite is a novel magnetic heterogeneous Fenton catalyst for the decolorization of synthetic dyes [15,16]. Meanwhile, $(Fe_{3-x}Ti_x)_{1-\delta}O_4$ is an excellent catalyst/sorbent for the oxidization and capture of elemental mercury from the flue gas [14].

Herein, non-stoichiometric Fe–Ti spinel was employed as an environmental-friendly catalyst for the SCR of NO with NH_3. At first, nanosized $(Fe_{3-x}Ti_x)_{1-\delta}O_4$ was synthesized using a co-precipitation method. Then, a packed-bed reactor system was used to investigate the SCR performance of $(Fe_{3-x}Ti_x)_{1-\delta}O_4$. At last, in situ DRIFTS study and kinetic analysis were employed to investigate the mechanism and structure–activity relationship of the SCR reaction over $(Fe_{3-x}Ti_x)_{1-\delta}O_4$.

2. Experimental

2.1. Catalyst preparation

Nanosized $Fe_{3-x}Ti_xO_4$, the precursor of $(Fe_{3-x}Ti_x)_{1-\delta}O_4$, was prepared using a co-precipitation method at room temperature,

* Corresponding authors. Tel.: +86 10 62771093; fax: +86 10 62771093.
E-mail addresses: lijunhua@tsinghua.edu.cn (J. Li), nqyan@sjtu.edu.cn (N. Yan).

0926-3373/$ – see front matter © 2012 Elsevier B.V. All rights reserved.
doi:10.1016/j.apcatb.2012.01.001

which was described in previous research [11,12,17]. γ-Fe_2O_3 ($Fe_{2.67}O_4$) and α-Fe_2O_3 were obtained after the thermal treatment of Fe_3O_4 under air for 3 h at 250 and 400 °C, respectively. $(Fe_{3-x}Ti_x)_{1-\delta}O_4$ ($x \neq 0$) was obtained after the thermal treatment of $Fe_{3-x}Ti_xO_4$ ($x \neq 0$) under air for 3 h at 400 °C.

Meanwhile, conventional vanadium-based catalyst (V_2O_5–WO_3/TiO_2) was prepared as a comparison [18]. V_2O_5–WO_3/TiO_2 catalyst with 1 wt.% V_2O_5 and 10 wt.% WO_3 were prepared by the conventional impregnation method using NH_4VO_3, $(NH_4)_{10}W_{12}O_{41}$ and $H_2C_2O_4{\cdot}2H_2O$ as precursors, and anatase TiO_2 as support. After the impregnation, excess water was removed in a rotary evaporator at 80 °C. Then, the sample calcined at 550 °C for 3 h under air.

2.2. Catalyst characterization

Crystal structure was determined using an X-ray diffractionmeter (Rigaku, D/max-2200/PC) between 20° and 70° at a step of 7° min^{-1} operating at 30 kV and 30 mA using Cu Kα radiation. BET surface area was determined using a nitrogen adsorption apparatus (Quantachrome, Autosorb-1). Catalyst was outgassed at 200 °C before BET measurement. H_2-TPR was recorded on a chemisorption analyzer (Micromeritics, ChemiSorb 2720 TPx) under a 10% hydrogen–90% nitrogen gas flow (50 cm^3 min^{-1}) at a rate of 10 °C min^{-1}. Temperature programmed desorption of ammonia (NH_3-TPD) was carried on another chemisorption analyzer (Micromeritics, AutoChem 2920). Before the experiment, about 0.15 g of catalyst was pretreated under He atmosphere at 300 °C for 60 min to remove the adsorbed H_2O and other gases. After the catalyst was cooled to 50 °C, the He flow was switched to a flow of 10% NH_3/He (15 mL min^{-1}) for 60 min. The sample was then purged by He (30 mL min^{-1}) for another 60 min. At last, NH_3-TPD was preformed at a heating rate of 10 °C min^{-1} to 600 °C under He atmosphere.

2.3. Catalytic test

The SCR reaction was evaluated in a fixed-bed quartz tube reactor (6 mm of internal diameter). The mass of $(Fe_{3-x}Ti_x)_{1-\delta}O_4$ with 40–60 mesh was 100 or 250 mg, and the total flow rate ranged from 100 to 400 mL min^{-1} (room temperature). The corresponding gas hourly space velocity (GHSV) was 2.4×10^4 to 2.4×10^5 cm^3 g^{-1} h^{-1}. A gas mixture containing 10% of H_2O (when used), 100 ppm of SO_2 (when used), 500 ppm of NO, 500 ppm of NH_3, 2% of O_2, and balance of N_2 was introduced into the reactor. The concentrations of NO_x (NO and NO_2), NH_3 and N_2O in the outlet were continually monitored by a chemiluminescent NO/NO_x analyzer (Thermo, Model 42*i*-HL) and a FTIR spectrometer (Gasmet FTIR DX4000), respectively. The determination precisions of gaseous NH_3, NO, NO_2 and N_2O were less than 2%.

As the SCR reaction reached the steady state, the ratio of NO conversion (X), N_2 selectivity (S) and the pseudo-first order rate constant (k) of the SCR reaction were calculated according to the following equations:

$$X = \frac{[NO]_{in} - [NO]_{out}}{[NO]_{in}} \times 100\% \quad (1)$$

$$S = 1 - \frac{[N_2O]_{out}}{[NO]_{in} - [NO]_{out}} \times 100\% \quad (2)$$

$$k = -\frac{F}{W} \ln(1 - X) \quad (3)$$

where $[NO]_{in}$ and $[NO]_{out}$ were the concentrations of gaseous NO in the inlet and outlet, respectively; $[N_2O]_{out}$ was the concentration of gaseous N_2O in the outlet; F was the total flow rate; and W was the mass of catalyst (g).

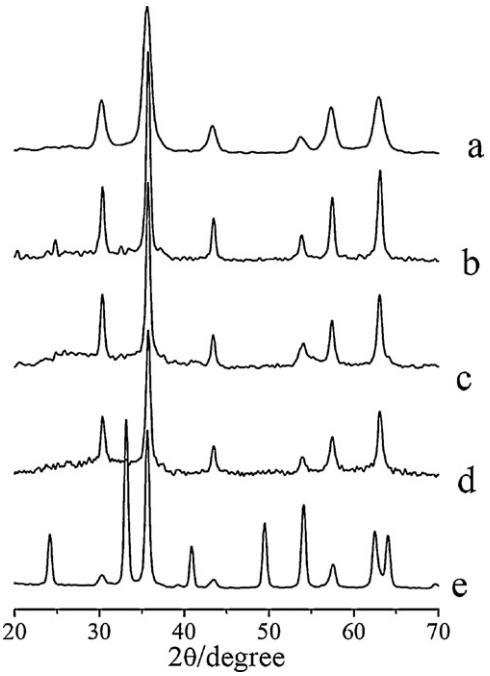

Fig. 1. XRD patterns of synthesized: (a) γ-Fe_2O_3; (b) $(Fe_{2.8}Ti_{0.2})_{0.87}O_4$; (c) $(Fe_{2.5}Ti_{0.5})_{0.84}O_4$; (d) $(Fe_2Ti)_{0.8}O_4$; and (e) α-Fe_2O_3.

2.4. In situ DRIFTS study

In situ DRIFT spectra were recorded on a Fourier transform infrared spectrometer (FTIR, Nicolet NEXUS 870) equipped with a liquid-nitrogen-cooled MCT detector, collecting 100 scans with a resolution of 4 cm^{-1}.

3. Results

3.1. Characterization

3.1.1. XRD

XRD patterns of synthesized catalysts are shown in Fig. 1. The characteristic peaks of $(Fe_{3-x}Ti_x)_{1-\delta}O_4$ corresponded very well to the standard card of maghemite (JCPDS: 39-1346), and the characteristic peaks corresponding to rutile and anatase did not appear. If there were some amorphous TiO_2 in synthesized $Fe_{3-x}Ti_xO_4$, it should transform to rutile (or anatase) after the calcination at 400 °C for 3 h [16]. Therefore, Ti was introduced into the spinel structure. Furthermore, electron energy loss spectroscopy (EELS), X-ray adsorption near edge structure (XANES) and extended X-ray adsorption fine structure (EXAFS) also demonstrated that Ti was incorporated into the spinel structure [11,12,17]. After the thermal treatment of Fe_3O_4 at 400 °C for 3 h, the characteristic peaks mainly corresponded to α-Fe_2O_3 (JCPDS: 33-0664). Meanwhile, a little γ-Fe_2O_3 still presented (at 30.5° and 43.3°).

BET surface areas of γ-Fe_2O_3, $(Fe_{2.8}Ti_{0.2})_{0.87}O_4$, $(Fe_{2.5}Ti_{0.5})_{0.84}O_4$, $(Fe_2Ti)_{0.8}O_4$ and α-Fe_2O_3 were 95.2, 47.5, 36.4, 85.2 and 48.3 m^2 g^{-1}, respectively.

3.1.2. H_2-TPR

H_2-TPR technique can be employed to study the reducibility [19]. TPR profiles of $(Fe_{3-x}Ti_x)_{1-\delta}O_4$ generally showed two obvious reduction peaks (shown in Fig. 2). The first set of peaks centered at about 318/450 °C corresponded to the reduction of $(Fe_{3-x}Ti_x)_{1-\delta}O_4$ to $Fe_{3-x}Ti_xO_4$ [20], and the set of broad peaks at higher temperature were attributed to the reduction of $Fe_{3-x}Ti_xO_4$ to Fe^0 and TiO_2 [20,21]. After the incorporation of Ti, a strong displacement of the

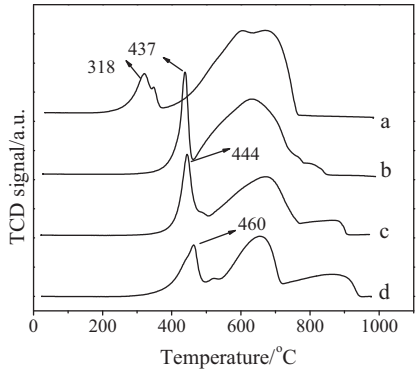

Fig. 2. H_2-TPR profiles of $(Fe_{3-x}Ti_x)_{1-\delta}O_4$: (a) $x = 0$; (b) $x = 0.2$; (c) $x = 0.5$; and (d) $x = 1$.

first reduction peak to about 450 °C happened in the TPR profiles. It indicates that the oxidative ability of Fe^{3+} cation on γ-Fe_2O_3 was much more than those of $(Fe_{3-x}Ti_x)_{1-\delta}O_4$ ($x \neq 0$).

The reduction of $(Fe_{3-x}Ti_x)_{1-\delta}O_4$ can be described as follows:

$$(Fe_{3-x}Ti_x)_{1-\delta}O_4 + \frac{36-12x}{9+x}H_2 \rightarrow \frac{24-8x}{9+x}Fe^0 + \frac{8x}{9+x}TiO_2 + \frac{36-12x}{9+x}H_2O \quad (4)$$

As shown in Table 1, H_2 consumption for $(Fe_{3-x}Ti_x)_{1-\delta}O_4$ reduction obviously decreased with the increase of Ti content in $(Fe_{3-x}Ti_x)_{1-\delta}O_4$, which is consistent with Reaction (4). However, the first step of $(Fe_{3-x}Ti_x)_{1-\delta}O_4$ reduction is as follows:

$$(Fe_{3-x}Ti_x)_{1-\delta}O_4 + \frac{4+4x}{9+x}H_2 \rightarrow \frac{8}{9+x}Fe_{3-x}Ti_xO_4 + \frac{4+4x}{9+x}H_2O \quad (5)$$

As shown in Reaction (5), H_2 consumption for the reduction of $(Fe_{3-x}Ti_x)_{1-\delta}O_4$ to $Fe_{3-x}Ti_xO_4$ would obviously increase with the increase of Ti content, which was demonstrated by TPR analysis (shown in Table 1). The SCR reaction is often operated below 500 °C, so the oxidation–reduction reaction happened on $(Fe_{3-x}Ti_x)_{1-\delta}O_4$ during the SCR reaction may be only related to the reduction of $(Fe_{3-x}Ti_x)_{1-\delta}O_4$ to $Fe_{3-x}Ti_xO_4$. As a result, the amount of reducible Fe^{3+} cation on $(Fe_{3-x}Ti_x)_{1-\delta}O_4$ for the SCR reaction increased with the increase of Ti content, although the oxidative ability of Fe^{3+} cation on $(Fe_{3-x}Ti_x)_{1-\delta}O_4$ decreased.

3.1.3. NH_3-TPD

Fig. 3 shows the results of NH_3-TPD over $(Fe_{3-x}Ti_x)_{1-\delta}O_4$. All of $(Fe_{3-x}Ti_x)_{1-\delta}O_4$ showed two obvious NH_3 desorption peaks. The peak centered at about 100 °C was caused by the desorption of physisorbed NH_3. The peak centered at about 400 °C was caused by the desorption of ionic NH_4^+ bound to the Brønsted acid sites and coordinated NH_3 bound to the Lewis acid sites. The amount of NH_3 adsorbed on $(Fe_{3-x}Ti_x)_{1-\delta}O_4$ at different temperature (saturated) can be approximately calculated according to the NH_3-TPD profiles. As shown in Table 2, the amount of NH_3 adsorbed on $(Fe_{3-x}Ti_x)_{1-\delta}O_4$ obviously increased after the incorporation of Ti into the spinel structure. Especially at high temperatures

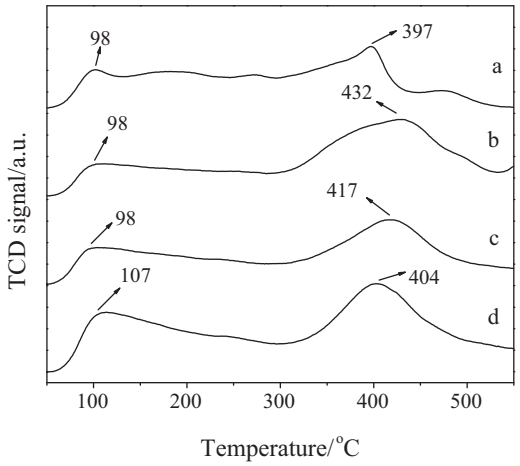

Fig. 3. NH_3-TPD profiles of $(Fe_{3-x}Ti_x)_{1-\delta}O_4$: (a) $x = 0$; (b) $x = 0.2$; (c) $x = 0.5$; and (d) $x = 1$.

(300–400 °C), the amounts of NH_3 adsorbed on $(Fe_{3-x}Ti_x)_{1-\delta}O_4$ ($x \neq 0$) were much more than those on γ-Fe_2O_3.

3.2. Catalytic performance

3.2.1. SCR activity

The ratio of NO conversion over synthesized catalysts as a function of reaction temperature is shown in Fig. 4a. NO conversion over α-Fe_2O_3 was about 70% at 250–300 °C and less than 40% at 150–200 and 300–400 °C, which was much less than that over γ-Fe_2O_3. At 150–250 °C, NO conversion over γ-Fe_2O_3 was much more than those over $(Fe_{3-x}Ti_x)_{1-\delta}O_4$ ($x \neq 0$). Because γ-Fe_2O_3 gradually transformed to α-Fe_2O_3, the SCR reaction over γ-Fe_2O_3 above 300 °C was difficult to reach the steady state and the ratio of NO conversion gradually decreased with the increase of reaction time. (The data shown in Fig. 4a were taken at 30 min.) The ratios of NO conversion over $(Fe_2Ti)_{0.8}O_4$ and $(Fe_{2.8}Ti_{0.2})_{0.87}O_4$ were higher than that of V_2O_5–WO_3/TiO_2, and they were more than 95% at 300–400 °C. $(Fe_{3-x}Ti_x)_{1-\delta}O_4$ showed an excellent N_2 selectivity (>96%), but some N_2O formed over V_2O_5–WO_3/TiO_2 above 300 °C (shown in Fig. 4b). Therefore, the SCR performance of $(Fe_2Ti)_{0.8}O_4$ was much better than that of conventional vanadium-based catalyst.

Then, the pseudo-first order rate constant (k) of the SCR reaction is calculated using Eq. (3). As shown in Table 3, k increased in the following sequence: $(Fe_{2.5}Ti_{0.5})_{0.84}O_4 < V_2O_5$–$WO_3$/$TiO_2 < (Fe_{2.8}Ti_{0.2})_{0.87}O_4 < (Fe_2Ti)_{0.8}O_4$. Although k of γ-Fe_2O_3 and α-Fe_2O_3 at 150–200 °C were more than that of $(Fe_2Ti)_{0.8}O_4$, k of $(Fe_2Ti)_{0.8}O_4$ above 300 °C was much more than those of γ-Fe_2O_3 and α-Fe_2O_3.

With the decrease of GHSV from 2.4×10^5 to 2.4×10^4 $cm^3\ g^{-1}\ h^{-1}$, the ratio of NO conversion over $(Fe_2Ti)_{0.8}O_4$ increased especially at 150–250 °C (shown in Fig. 5). As the GHSV was 2.4×10^4 $cm^3\ g^{-1}\ h^{-1}$, the ratio of NO conversion over $(Fe_2Ti)_{0.8}O_4$ can reach 90% at 200 °C and near 100% above 250 °C.

Table 1
H_2 consumption for $(Fe_{3-x}Ti_x)_{1-\delta}O_4$ reduction resulted from H_2-TPR profiles (mmol g^{-1}).

	Total H_2 consumption	H_2 consumption of the first reduction peak
γ-Fe_2O_3	19 ± 1	2.1 ± 0.1
$(Fe_{2.8}Ti_{0.2})_{0.87}O_4$	17 ± 1	2.7 ± 0.1
$(Fe_{2.5}Ti_{0.5})_{0.84}O_4$	15 ± 1	2.9 ± 0.2
$(Fe_2Ti)_{0.8}O_4$	12 ± 1	3.5 ± 0.2

Table 2
The amount of NH_3 adsorbed on $(Fe_{3-x}Ti_x)_{1-\delta}O_4$ at different temperatures (mmol g^{-1}).

	50 °C	200 °C	300 °C	400 °C
γ-Fe_2O_3	0.66 ± 0.03	0.46 ± 0.02	0.31 ± 0.02	0.11 ± 0.01
$(Fe_{2.8}Ti_{0.2})_{0.87}O_4$	0.86 ± 0.04	0.67 ± 0.03	0.57 ± 0.03	0.35 ± 0.02
$(Fe_{2.5}Ti_{0.5})_{0.84}O_4$	0.71 ± 0.04	0.52 ± 0.03	0.42 ± 0.02	0.26 ± 0.01
$(Fe_2Ti)_{0.8}O_4$	1.0 ± 0.05	0.73 ± 0.04	0.60 ± 0.03	0.39 ± 0.02

Table 3
Pseudo-first order rate constant (k) of the SCR reaction over α-Fe_2O_3, $(Fe_{3-x}Ti_x)_{1-\delta}O_4$ and V_2O_5–WO_3/TiO_2 ($cm^3\ g^{-1}\ s^{-1}$).

	150 °C	200 °C	250 °C	300 °C	350 °C	400 °C
α-Fe_2O_3	4.6 ± 4.6	34.6 ± 7.2	72.5 ± 11	81.3 ± 12	26.8 ± 5.4	–
γ-Fe_2O_3	12.8 ± 6.4	51.3 ± 9	135 ± 13	180 ± 18	185 ± 19	69.0 ± 11
$(Fe_{2.8}Ti_{0.2})_{0.87}O_4$	1.6 ± 1.6	11.2 ± 5.6	65.0 ± 10	192 ± 19	>322	>348
$(Fe_{2.5}Ti_{0.5})_{0.84}O_4$	0.5 ± 0.5	2.6 ± 2.6	23.5 ± 4.7	103 ± 13	224 ± 22	294 ± 29
$(Fe_2Ti)_{0.8}O_4$	2.1 ± 2.1	17.2 ± 8.6	88.8 ± 12	251 ± 25	>322	>348
V_2O_5–WO_3/TiO_2	1.0 ± 1.0	7.4 ± 7.4	50.9 ± 9	162 ± 16	>322	>348

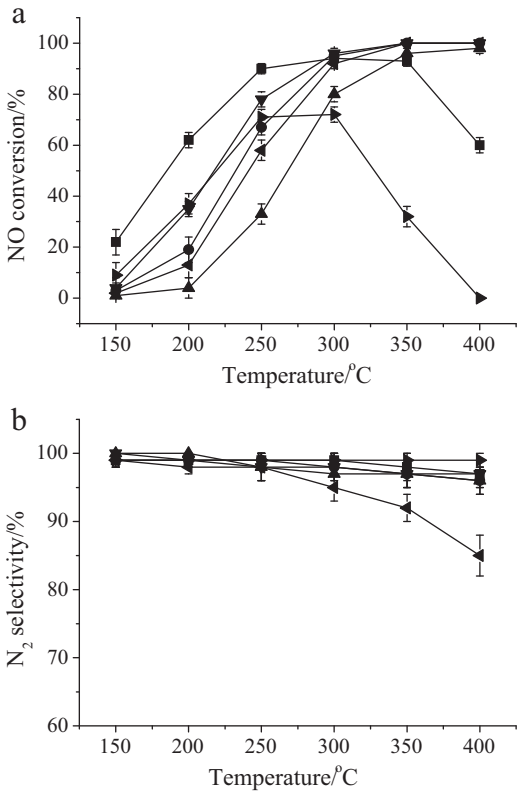

Fig. 4. SCR performance of synthesized catalysts: (a) NO conversion; (b) N_2 selectivity. ■, γ-Fe_2O_3; ●, $(Fe_{2.8}Ti_{0.2})_{0.87}O_4$; ▲, $(Fe_{2.5}Ti_{0.5})_{0.84}O_4$; ▼, $(Fe_2Ti)_{0.8}O_4$; ◄, V_2O_5–WO_3/TiO_2; ►, α-Fe_2O_3. Reaction condition: [NO] = [NH_3] = 500 ppm, [O_2] = 2%, catalyst mass = 100 mg, total flow rate = 200 mL min^{-1}, GHSV = 120,000 $cm^3\ g^{-1}\ h^{-1}$.

3.2.2. *Effect of SO_2 and H_2O*

Water vapor and SO_2 in the flue gas often lead to the deactivation of SCR catalyst [22–25]. Therefore, the effect of 10% of H_2O and 100 ppm of SO_2 on the SCR activity of $(Fe_2Ti)_{0.8}O_4$ was investigated with a 24 h test. As shown in Fig. 6a, the presence of H_2O and SO_2 showed a severe interference with the SCR reaction over $(Fe_2Ti)_{0.8}O_4$ at 150–250 °C. However, the temperature of flue gas at the SCR unit of coal-fired power plant is about 300–400 °C. The ratio of NO conversion over $(Fe_2Ti)_{0.8}O_4$ in the presence of H_2O and SO_2 can reach 90% at 300 °C and near 100% above 350 °C, which was close to that of V_2O_5–WO_3/TiO_2 (shown in Fig. 6b). It indicates that $(Fe_2Ti)_{0.8}O_4$ had an excellent H_2O and SO_2 durability in the temperature range of the SCR unit of coal-fired power plant.

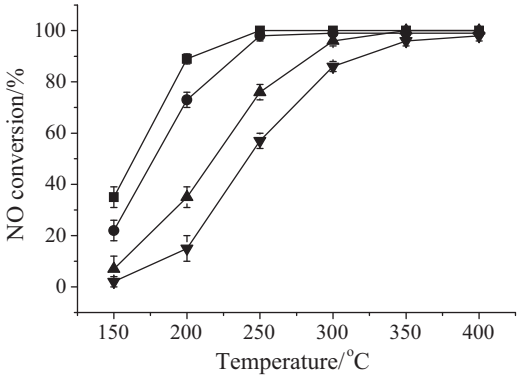

Fig. 5. Influence of GHSV on NO conversion over $(Fe_2Ti)_{0.8}O_4$, [NO] = [NH_3] = 500 ppm, [O_2] = 2%, GHSV: ■, 24,000; ●, 60,000; ▲, 120,000; ▼, 240,000 $cm^3\ g^{-1}\ h^{-1}$.

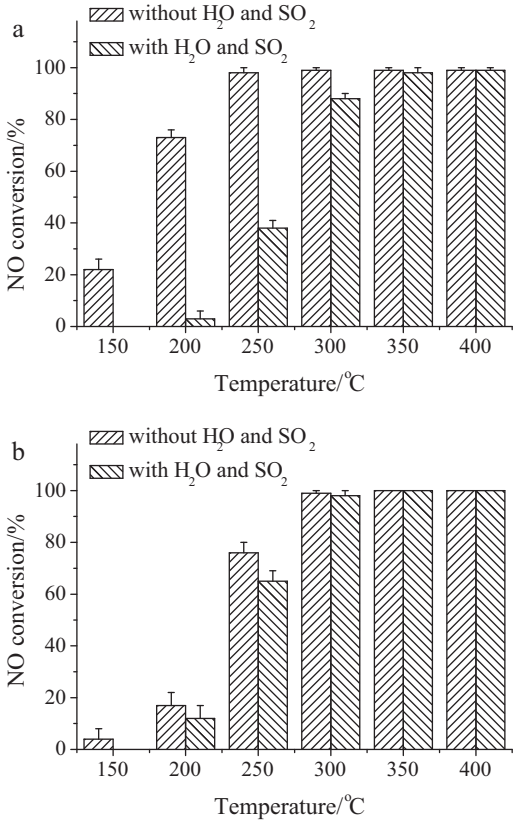

Fig. 6. Effect of 10% of H_2O and 100 ppm of SO_2 on the SCR reaction over: (a) $(Fe_2Ti)_{0.8}O_4$; (b) V_2O_5–WO_3/TiO_2. Reaction condition: [NO] = [NH_3] = 500 ppm, [O_2] = 2%, catalyst mass = 100 mg, total flow rate = 100 mL min^{-1}, GHSV = 60,000 $cm^3\ g^{-1}\ h^{-1}$.

3.3. *DRIFT study*

After γ-Fe_2O_3 were treated with NH_3/N_2 at 200 °C, eight bands at 1680, 1620, 1560, 1450, 1400, 1320, 1280 and 1210 cm^{-1} appeared (shown in Fig. 7a). The bands at 1680 and 1450 cm^{-1} were assigned to ionic NH_4^+ bound to the Brønsted acid sites, and the band at 1210 cm^{-1} was attributed to coordinated NH_3 bound to the Lewis acid sites. The bands at 1560, 1400, 1320 and 1280 cm^{-1} may be attributed to the oxidization/deformation of adsorbed NH_3 [26]. The band at 1620 cm^{-1} may be assigned to adsorbed H_2O

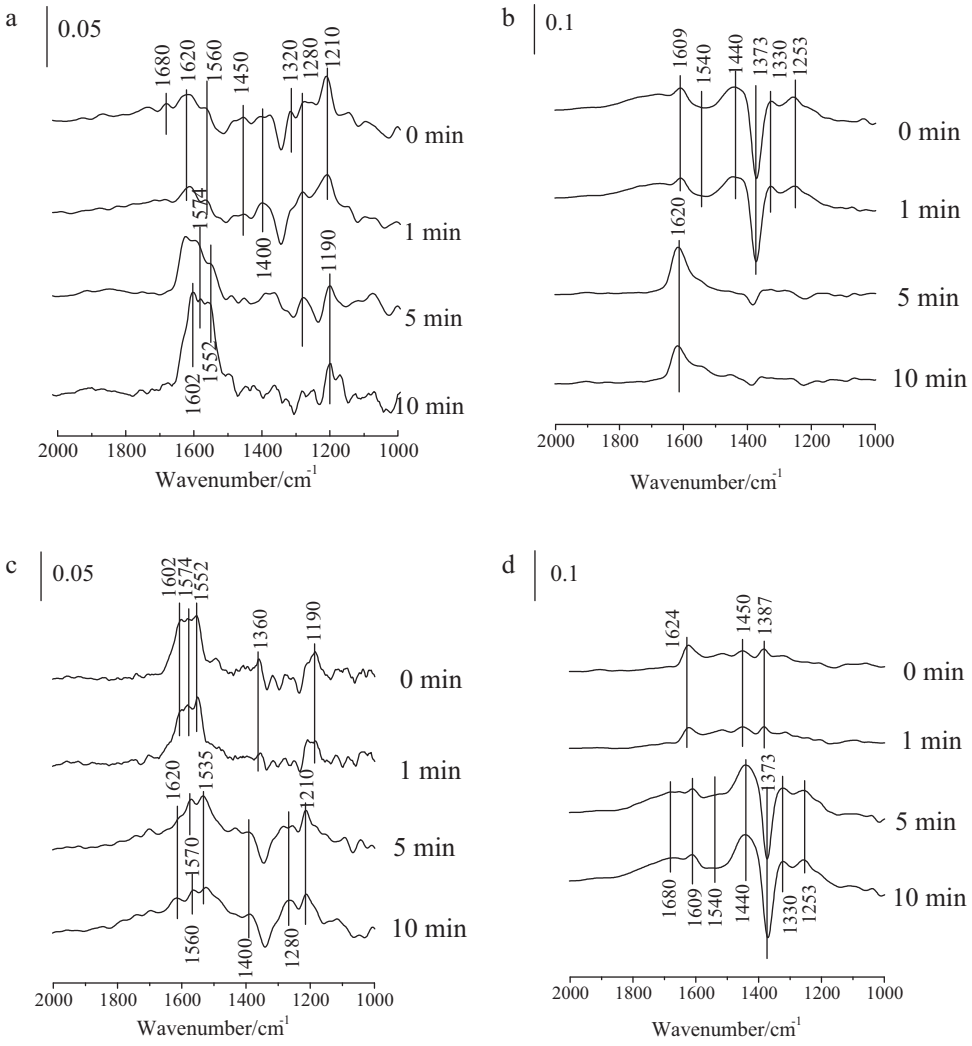

Fig. 7. DRIFT spectra taken at 200 °C upon passing NO + O_2 over NH_3 presorbed: (a) γ-Fe_2O_3; (b) $(Fe_2Ti)_{0.8}O_4$. DRIFT spectra taken at 200 °C upon passing NH_3 over NO + O_2 presorbed: (c) γ-Fe_2O_3; (d) $(Fe_2Ti)_{0.8}O_4$.

resulting from the oxidization of adsorbed NH_3. After $(Fe_2Ti)_{0.8}O_4$ was treated with NH_3/N_2 at 200 °C, four bands at 1609, 1440, 1330 and 1253 cm^{-1} appeared (shown in Fig. 7b). The band at 1440 cm^{-1} was assigned to ionic NH_4^+ bound to the Brønsted acid sites, and the bands at 1609 and 1253 cm^{-1} were attributed to coordinated NH_3 bound to the Lewis acid sites. The band at 1330 cm^{-1} may be attributed to the asymmetric deformation of coordinated NH_3 [26]. The negative bands at 1373 and 1540 cm^{-1} may be assigned to residual sulfate species in synthesized $(Fe_2Ti)_{0.8}O_4$, which was covered by NH_3. Comparing Fig. 7a with Fig. 7b, the band intensity of adsorbed NH_3 on $(Fe_2Ti)_{0.8}O_4$ was much more than that on γ-Fe_2O_3. It indicates that the adsorption of NH_3 was promoted due to the incorporation of Ti into γ-Fe_2O_3, which was consistent with the result of NH_3-TPD.

After γ-Fe_2O_3 were treated with NO + O_2/N_2 at 200 °C, five bands at 1602, 1574, 1552, 1360 and 1190 cm^{-1} appeared (shown in Fig. 7c). These bands were mainly attributed to monodentate nitrite [27,28]. After $(Fe_2Ti)_{0.8}O_4$ was treated with NO + O_2/N_2 at 200 °C, three slight bands at 1624, 1450 and 1387 cm^{-1} appeared (shown in Fig. 7d), which were also attributed to monodentate nitrite [27]. Comparing Fig. 7c with Fig. 7d, the band intensity of adsorbed NO_x on $(Fe_2Ti)_{0.8}O_4$ was much less than that on γ-Fe_2O_3. It indicates that the adsorption of NO_x was restrained due to the incorporation of Ti into γ-Fe_2O_3.

After NO + O_2/N_2 passed over NH_3 pretreated γ-Fe_2O_3 at 200 °C, both ionic NH_4^+ (at 1680 and 1450 cm^{-1}) and coordinated NH_3 (at 1210 cm^{-1}) diminished (shown in Fig. 7a). It indicates that the adsorbed ammonia species on γ-Fe_2O_3 can react with NO. After NO + O_2/N_2 passed over NH_3 pretreated γ-Fe_2O_3 for 10 min, γ-Fe_2O_3 was mainly covered by monodentate nitrite. After NH_3 passed over NO + O_2 pretreated γ-Fe_2O_3 at 200 °C, the bands corresponding to adsorbed nitrite gradually decreased (shown in Fig. 7c). It suggests that adsorbed nitrogen oxide can react with ammonia. Therefore, both the Eley–Rideal mechanism and the Langmuir–Hinshelwood mechanism may account for the SCR of NO with NH_3 over γ-Fe_2O_3, which was consistent with our previous research on $(Fe_{3-x}Mn_x)_{1-\delta}O_4$ [29].

After NO + O_2/N_2 passed over NH_3 pretreated $(Fe_2Ti)_{0.8}O_4$ at 200 °C, the band at 1440 cm^{-1} corresponding to ionic NH_4^+ and the bands at 1609, 1330 and 1253 cm^{-1} corresponding to coordinated NH_3 both diminished (shown in Fig. 7b). Meanwhile, a new band at 1620 cm^{-1} appeared. This band was assigned to adsorbed H_2O, which is the product of SCR reaction [26]. They both suggest that the adsorbed ammonia species on $(Fe_2Ti)_{0.8}O_4$ can react with NO. However, the bands corresponding to adsorbed nitrogen oxides can hardly be detected after NO + O_2/N_2 passed over NH_3 pretreated $(Fe_2Ti)_{0.8}O_4$. After NH_3 passed over NO + O_2 pretreated $(Fe_2Ti)_{0.8}O_4$, the bands at 1609, 1440, 1330 and 1253 cm^{-1} corresponding to

adsorbed ammonia species appeared (shown in Fig. 7d). However, the band at 1620 cm^{-1} corresponding to adsorbed H_2O can hardly be detected. It suggests that the reaction between ammonia and adsorbed nitrogen oxides on $(Fe_2Ti)_{0.8}O_4$ may be neglected. Therefore, the SCR reaction over $(Fe_2Ti)_{0.8}O_4$ mainly followed the Eley–Rideal mechanism.

4. Discussion

4.1. Kinetic study

The SCR reaction over $(Fe_{3-x}Ti_x)_{1-\delta}O_4$ through the Langmuir–Hinshelwood mechanism (i.e. reaction of adsorbed ammonia species with adsorbed NO_x species) can be approximately described as follows [28,30]:

$$NH_{3(g)} \leftrightharpoons NH_{3(ad)} \quad (6)$$

$$NO_{(g)} \leftrightharpoons NO_{(ad)} \quad (7)$$

$$\equiv Fe^{3+} + O^{2-} + NO_{(ad)} \rightarrow \equiv Fe^{2+} + NO_2^- \quad (8)$$

$$NO_2^- + NH_{3(ad)} \rightarrow N_2 + H_2O + OH^- \quad (9)$$

$$\equiv Fe^{2+} + \frac{1}{4}O_2 \rightarrow \equiv Fe^{3+} + \frac{1}{2}\equiv O^{2-} \quad (10)$$

The SCR reaction over $(Fe_{3-x}Ti_x)_{1-\delta}O_4$ through the Eley–Rideal mechanism (i.e. reaction of activated ammonia with gaseous NO) can be approximately described as follows [30]:

$$NH_{3(g)} \leftrightharpoons NH_{3(ad)} \quad (6)$$

$$NH_{3(ad)} + \equiv Fe^{3+} \rightarrow -NH_2^+ + \equiv Fe^{2+} + H^+ \quad (11)$$

$$-NH_2 + NO_{(g)} \rightarrow N_2 + H_2O \quad (12)$$

$$\equiv Fe^{2+} + \frac{1}{4}O_2 \rightarrow \equiv Fe^{3+} + \frac{1}{2}\equiv O^{2-} \quad (10)$$

Because the adsorption of NO and NH_3 was saturated at the steady state, both the concentration of NH_3 adsorbed on the surface ($[NH_{3(ad)}]$) and the concentration of NO adsorbed on the surface ($[NO_{(ad)}]$) at a specific temperature can be regarded as constants. Reactions (6) and (7) were both exothermic reactions, so $[NH_{3(ad)}]$ and $[NO_{(ad)}]$ would rapidly decrease with the increase of reaction temperature.

The kinetic equation of the oxidization of adsorbed NO by Fe^{3+} cations on the surface (Reaction (8)) can be described as:

$$-\frac{d[NO_{(ad)}]}{dt} = -\frac{d[Fe^{3+}]}{dt} = \frac{d[NO_2^-]}{dt} = k_1'[NO_{(ad)}][Fe^{3+}] \quad (13)$$

where k_1', $[NO_2^-]$ and $[Fe^{3+}]$ were the kinetic constant of Reaction (8), the concentrations of NO_2^- and reducible Fe^{3+} on the surface, respectively.

If the surface was saturated with the chemical adsorption of NO_2^-, $[NO_2^-]$ may be regarded as a constant and approximately proportional to the product of $[NO_{(ad)}]$ and $[Fe^{3+}]$. Therefore, $[NO_2^-]$ at the steady state can be approximately described as:

$$[NO_2^-] = k_1[NO_{(ad)}][Fe^{3+}] \quad (14)$$

where k_1 was a constant. Reaction (8) is the oxidization of adsorbed NO, so k_1 was related to the oxidative ability of Fe^{3+} on the surface.

The kinetic equation of the reaction of adsorbed ammonia species with adsorbed NO_x species (Reaction (9)) can be described as:

$$-\frac{d[NO_2^-]}{dt} = -\frac{d[NH_{3(ad)}]}{dt} = \frac{d[N_2]}{dt} = k_2[NO_2^-][NH_{3(ad)}] = k_1k_2[NO_{(ad)}][Fe^{3+}][NH_{3(ad)}] \quad (15)$$

where k_2 was the kinetic constant of Reaction (9).

Then, the reduction of gaseous NO by the whole catalyst column through the Langmuir–Hinshelwood mechanism can be described as:

$$-\frac{d[NO_{(g)}]}{dt}_{L-H} = k_1k_2[NO_{(ad)}][Fe^{3+}][NH_{3(ad)}]t' \quad (16)$$

where t' was the time how long the gas pass through the catalyst column. t' was equal to the ratio of the volume of the whole catalyst column to the flow rate, which was related to the reciprocal of GHSV. If the SCR reaction mainly followed the Langmuir–Hinshelwood mechanism, the reaction orders with respect to the concentrations of gaseous NH_3 and NO were both zero (shown in Eq. (16)).

The kinetic equation of the activation of adsorbed NH_3 (Reaction (11)) can be described as:

$$-\frac{d[NH_{3(ad)}]}{dt} = -\frac{d[Fe^{3+}]}{dt} = \frac{d[-NH_2]}{dt} = k_3'[NH_{3(ad)}][Fe^{3+}] \quad (17)$$

where k_3' was the kinetic constant of Reaction (11).

If the surface was saturated with the chemical adsorption of $-NH_2$, $[-NH_2]$ may be regarded as a constant and approximately proportional to the product of $[NH_{3(ad)}]$ and $[Fe^{3+}]$. Therefore, $[-NH_2]$ at the steady state can be approximately described as:

$$[-NH_2] = k_3[NH_{3(ad)}][Fe^{3+}] \quad (18)$$

where k_3 was a constant. Reaction (11) is the activation (oxidization) of adsorbed NH_3, so k_3 was related to the oxidative ability of Fe^{3+} on the surface.

The kinetic equation of the reduction of gaseous NO by activated NH_3 (Reaction (12)) can be described as:

$$-\frac{d[-NH_2]}{dt} = -\frac{d[NO_{(g)}]}{dt} = \frac{d[N_2]}{dt} = k_4[-NH_2][NO_{(g)}] \quad (19)$$

where k_4 was the kinetic constant of Reaction (12).

Besides Reaction (12), Reactions (7)–(9) also contributed to the reduction of gaseous NO. Therefore, the kinetic equation of gaseous NO reduction should be described as:

$$-\frac{d[NO_{(g)}]}{dt} = k_4[-NH_2][NO_{(g)}] + k_1k_2[NO_{(ad)}][Fe^{3+}][NH_{3(ad)}] \quad (20)$$

If the SCR reaction mainly followed the Eley–Rideal mechanism, the effect of the SCR reaction through the Langmuir–Hinshelwood mechanism on that through the Eley–Rideal mechanism can be approximately neglected. Therefore, the concentration of gaseous NO at the specific section of catalyst column ($[NO_{(g)}]_l$) can be approximately described as:

$$[NO_{(g)}]_l = [NO_{(g)}]_{in} \exp(-k_4[-NH_2]l) = [NO_{(g)}]_{in} \exp(-k_3k_4[NH_{3(ad)}][Fe^{3+}]l) \quad (21)$$

where l was the time how long gaseous NO reached the specific section of catalyst column.

After the incorporation of Eqs. (18) and (21) into Eq. (19), the formed N_2 over the specific section of catalyst column can be described as:

$$\frac{d[N_2]_l}{dt} = k_3k_4[Fe^{3+}][NH_{3(ad)}][NO_{(g)}]_{in} \exp(-k_3k_4[Fe^{3+}][NH_{3(ad)}]l) \quad (22)$$

After the integration, the amount of N_2 formed over the whole catalyst column can be described as:

$$\frac{d[N_2]}{dt} = k_3k_4[Fe^{3+}][NH_{3(ad)}][NO_{(g)}]_{in} \int_0^{t'} \exp(-k_3k_4[Fe^{3+}][NH_{3(ad)}]l)\ dl \quad (23)$$

Therefore, the reduction of NO by the whole catalyst column through the Eley–Rideal mechanism can be approximately described as:

$$-\frac{d[NO_{(g)}]}{dt}_{E-R} = k_3k_4[Fe^{3+}][NH_{3(ad)}][NO_{(g)}]_{in} \int_0^{t'} \exp(-k_3k_4[Fe^{3+}][NH_{3(ad)}]l)\ dl \quad (24)$$

If the SCR reaction mainly followed the Eley–Rideal mechanism, the reaction orders with respect to the concentrations of gaseous NH_3 and NO were 0 and 1, respectively (shown in Eq. (24)).

Taking into account of both the Eley–Rideal mechanism and the Langmuir–Hinshelwood mechanism, the kinetic equation of the SCR reaction over Fe–Ti spinel can be described as:

$$-\frac{d[NO_{(g)}]}{dt} = k_1k_2[NO_{(ad)}][Fe^{3+}][NH_{3(ad)}]t' + k_3k_4[Fe^{3+}][NH_{3(ad)}][NO_{(g)}]_{in} \int_0^{t'} \exp(-k_3k_4[Fe^{3+}][NH_{3(ad)}]l)\ dl \quad (25)$$

Meanwhile, the ratio of NO conversion can be described as:

$$X = k_1k_2\frac{[NO_{(ad)}]}{[NO_{(g)}]_{in}}[Fe^{3+}][NH_{3(ad)}]t' + k_3k_4[Fe^{3+}][NH_{3(ad)}] \int_0^{t'} \exp(-k_3k_4[Fe^{3+}][NH_{3(ad)}]l)\ dl \quad (26)$$

If the reaction order with respect to the concentration of gaseous NO was 1, the SCR reaction over $(Fe_{3-x}Ti_x)_{1-\delta}O_4$ would mainly follow the Eley–Rideal mechanism. If the reaction order with respect to the concentration of gaseous NO was 0, the SCR reaction over $(Fe_{3-x}Ti_x)_{1-\delta}O_4$ would mainly follow the Langmuir–Hinshelwood mechanism. If the reaction order with respect to the concentration of gaseous NO was 0–1, both the Eley–Rideal mechanism and the Langmuir–Hinshelwood mechanism would contribute to the SCR reaction over $(Fe_{3-x}Ti_x)_{1-\delta}O_4$. To determine the reaction order with respect to the concentration of gaseous NO, the concentration of gaseous NO varied from 500 to 1500 ppm, in which the ratio of NH_3 to NO was kept constantly at 1 [29]. Because the SCR reaction over γ-Fe_2O_3 above 300 °C was difficult to reach the steady state, the test over γ-Fe_2O_3 was operated at 150–250 °C. After doubling NO concentration, the ratio of NO conversion over γ-Fe_2O_3 obviously decreased (shown in Fig. 8a). But the ratio of NO conversion did not halve at 200–250 °C. It indicates that the order of SCR reaction over γ-Fe_2O_3 with respect to the concentration of gaseous NO was less than 1, but it was more than 0. Therefore, both the Eley–Rideal mechanism and the Langmuir–Hinshelwood mechanism contributed to the SCR reaction over γ-Fe_2O_3. However, little decrease of the ratio of NO conversion can be observed after varying gaseous NO concentration of the SCR reaction over $(Fe_2Ti)_{0.8}O_4$ (shown in Fig. 8b). It indicates that the order of SCR reaction over $(Fe_2Ti)_{0.8}O_4$ with respect to the concentration of gaseous NO was 1. Therefore, the SCR reaction over $(Fe_2Ti)_{0.8}O_4$ mainly followed the Eley–Rideal mechanism. These results were consistent with the results of in situ DRIFT analysis.

4.2. Structure–activity relationship

k_1 and k_3 were related to the oxidative ability of Fe^{3+} on the surface, which depended on the reaction temperature. TPR analysis demonstrated that the oxidative ability of Fe^{3+} cation on

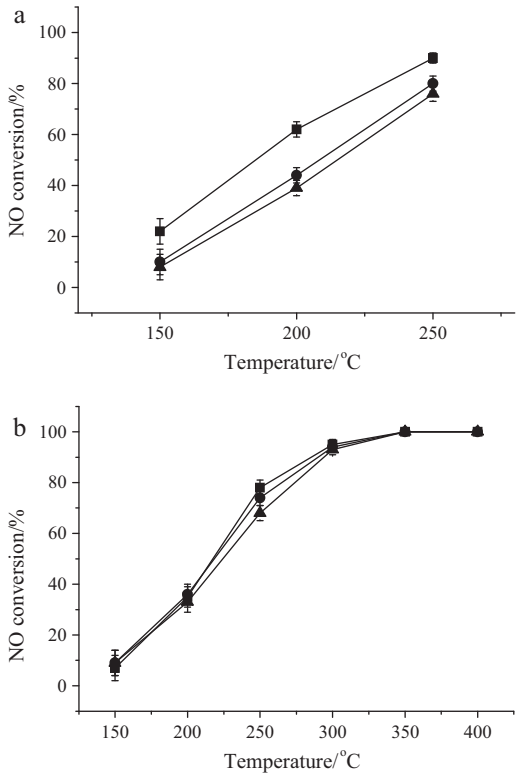

Fig. 8. Influence of the concentration of gaseous NO on NO conversion, $[O_2]$ = 2%, catalyst mass = 100 mg, total flow rate = 200 mL min^{-1}, GHSV = 120,000 cm^3 g^{-1} h^{-1}, [NO] = [NH_3]: ■, 500; ●, 1000; ▲, 1500 ppm. (a) γ-Fe_2O_3; (b) $(Fe_2Ti)_{0.8}O_4$.

γ-Fe_2O_3 was much better than those on $(Fe_{3-x}Ti_x)_{1-\delta}O_4$. Therefore, k_1 and k_3 of γ-Fe_2O_3 were larger than those of $(Fe_{3-x}Ti_x)_{1-\delta}O_4$. With the increase of reaction temperature, their difference would decrease.

As k_1 decreased due to the incorporation of Ti into γ-Fe_2O_3, the chemical adsorption of NO_2^- on $(Fe_{3-x}Ti_x)_{1-\delta}O_4$ was restrained (hinted by Eq. (14)), which was demonstrated by the DRIFT study (shown in Fig. 7). The adsorption of NH_3 was promoted due to the incorporation of Ti into γ-Fe_2O_3 (shown in Table 2), so gaseous NH_3 may compete with gaseous NO for the active sites. As a result, the Langmuir–Hinshelwood mechanism was restrained due to the incorporation of Ti.

Because the Langmuir–Hinshelwood mechanism contributed to the SCR reaction over γ-Fe_2O_3, the SCR activity of γ-Fe_2O_3 was better than those of $(Fe_{3-x}Ti_x)_{1-\delta}O_4$ ($x \neq 0$) at 150–250 °C. At 300–400 °C, the SCR reaction over γ-Fe_2O_3 may mainly follow the Eley–Rideal mechanism. Although k_3 of γ-Fe_2O_3 was larger than those of $(Fe_{3-x}Ti_x)_{1-\delta}O_4$ ($x \neq 0$), both the concentration of reducible Fe^{3+} (shown in Table 1) and the concentration of NH_3 adsorbed (shown in Table 2) on γ-Fe_2O_3 were much less than those on $(Fe_{3-x}Ti_x)_{1-\delta}O_4$ ($x \neq 0$). Furthermore, γ-Fe_2O_3 is metastable, and converts quickly to α-Fe_2O_3 above 300 °C [13], which has a poor SCR activity (shown in Fig. 4a). As a result, the SCR activity of γ-Fe_2O_3 at 300–400 °C was generally much less than those of $(Fe_{3-x}Ti_x)_{1-\delta}O_4$ ($x \neq 0$) (shown in Fig. 4a).

The introduction of Ti had a stabilization effect on the spinel structure and the phase transition temperature of Ti-containing maghemite to Ti-containing hematite shifted to high temperature with the increase of Ti content in $(Fe_{3-x}Ti_x)_{1-\delta}O_4$ [16]. Therefore, the phase transition of $(Fe_{3-x}Ti_x)_{1-\delta}O_4$ ($x \neq 0$) cannot happen below 400 °C.

The SCR reaction over $(Fe_{3-x}Ti_x)_{1-\delta}O_4$ ($x \neq 0$) mainly followed the Eley–Rideal mechanism. Therefore, the ratio of NO

conversion over $(Fe_{3-x}Ti_x)_{1-\delta}O_4$ ($x \neq 0$) was approximately proportional to the product of the oxidative ability of Fe^{3+} cation on the surface (k_3), the concentration of NH_3 adsorbed on the surface ($[NH_{3(ad)}]$) and the concentration of reducible Fe^{3+} cation on the surface ($[Fe^{3+}]$) (hinted by Eq. (24)). As shown in Fig. 2, the first reduction peak of $(Fe_{3-x}Ti_x)_{1-\delta}O_4$ ($x \neq 0$) slightly shifted to high temperature with the increase of Ti content in $(Fe_{3-x}Ti_x)_{1-\delta}O_4$. It indicates that k_3 slightly decreased with the increase of Ti in $(Fe_{3-x}Ti_x)_{1-\delta}O_4$. $[Fe^{3+}][NH_{3(ad)}]$ on $(Fe_{3-x}Ti_x)_{1-\delta}O_4$ ($x \neq 0$) (resulted from the product of the data in Tables 1 and 2) obviously increased in the following sequence: $(Fe_{2.5}Ti_{0.5})_{0.84}O_4 < (Fe_{2.8}Ti_{0.2})_{0.87}O_4 < (Fe_2Ti)_{0.8}O_4$. As a result, the SCR activity of $(Fe_{3-x}Ti_x)_{1-\delta}O_4$ ($x \neq 0$) increased in the same sequence: $(Fe_{2.5}Ti_{0.5})_{0.84}O_4 < (Fe_{2.8}Ti_{0.2})_{0.87}O_4 < (Fe_2Ti)_{0.8}O_4$.

5. Conclusion

A series of SCR catalysts $(Fe_{3-x}Ti_x)_{1-\delta}O_4$ were synthesized using a co-precipitation method. Because the SCR reaction over $(Fe_{3-x}Ti_x)_{1-\delta}O_4$ through the Langmuir–Hinshelwood mechanism was restrained due to the incorporation of Ti into γ-Fe_2O_3, the SCR activity of $(Fe_{3-x}Ti_x)_{1-\delta}O_4$ ($x \neq 0$) was much less than that of γ-Fe_2O_3 at 150–250 °C. Because both the concentration of NH_3 adsorbed and the concentration of reducible Fe^{3+} cation on $(Fe_{3-x}Ti_x)_{1-\delta}O_4$ increased due to the incorporation of Ti into γ-Fe_2O_3, the SCR reaction over $(Fe_{3-x}Ti_x)_{1-\delta}O_4$ through the Eley–Rideal mechanism was promoted. Therefore, the SCR activity of $(Fe_{3-x}Ti_x)_{1-\delta}O_4$ ($x \neq 0$) was much better than that of γ-Fe_2O_3 at 300–400 °C. $(Fe_2Ti)_{0.8}O_4$ showed excellent SCR activity, N_2 selectivity and H_2O/SO_2 durability at 300–400 °C, so it may be an environmental-friendly and low-cost catalyst to substitute the conventional vanadium-based catalyst.

Acknowledgments

This study was financially supported by the National Natural Science Fund of China (Grant No. 51078203), the National High-Tech Research and Development (863) Program of China (Grant Nos. 2010AA065002 and 2009AA06Z301) and the Scholarship Award for Excellent Doctoral Student granted by Ministry of Education of China.

References

[1] G.S. Qi, R.T. Yang, Appl. Catal. B-Environ. 44 (2003) 217–225.
[2] N.Y. Topsoe, Science 265 (1994) 1217–1219.
[3] G.S. Qi, R.T. Yang, R. Chang, Appl. Catal. B-Environ. 51 (2004) 93–106.
[4] R.Q. Long, R.T. Yang, J. Am. Chem. Soc. 121 (1999) 5595–5596.
[5] J.P. Chen, M.C. Hausladen, R.T. Yang, J. Catal. 151 (1995) 135–146.
[6] F.D. Liu, K. Asakura, H. He, W.P. Shan, X.Y. Shi, C.B. Zhang, Appl. Catal. B-Environ. 103 (2010) 369–377.
[7] F. Liu, H. He, C. Zhang, Chem. Commun. 17 (2008) 2043–2045.
[8] F.D. Liu, H. He, Y. Ding, C.B. Zhang, Appl. Catal. B-Environ. 93 (2009) 194–204.
[9] F.D. Liu, H. He, C.B. Zhang, Z.C. Feng, L.R. Zheng, Y.N. Xie, T.D. Hu, Appl. Catal. B-Environ. 96 (2010) 408–420.
[10] F.D. Liu, H. He, J. Phys. Chem. C 114 (2010) 16929–16936.
[11] N. Millot, D. Aymes, F. Bernard, J.C. Niepce, A. Traverse, F. Bouree, B.L. Cheng, P. Perriat, J. Phys. Chem. B 107 (2003) 5740–5750.
[12] P. Perriat, E. Fries, N. Millot, B. Domenichini, Solid State Ionics 117 (1999) 175–184.
[13] R.M. Cornell, U. Schwertmann, The Iron Oxides: Structure, Properties, Reactions, Occurrences and Uses, Wiley-VCH, New York, 2003.
[14] S. Yang, Y. Guo, N. Yan, D. Wu, H. He, Z. Qu, C. Yang, Q. Zhou, J. Jia, ACS Appl. Mater. Interfaces 3 (2011) 209–217.
[15] S.J. Yang, H.P. He, D.Q. Wu, D. Chen, Y.H. Ma, X.L. Li, J.X. Zhu, P. Yuan, Ind. Eng. Chem. Res. 48 (2009) 9915–9921.
[16] S. Yang, H. He, D. Wu, D. Chen, X. Liang, Z. Qin, M. Fan, J. Zhu, P. Yuan, Appl. Catal. B-Environ. 89 (2009) 527–535.
[17] N. Guigue-Millot, Y. Champion, M.J. Hytch, F. Bernard, S. Begin-Colin, P. Perriat, J. Phys. Chem. B 105 (2001) 7125–7132.
[18] L.A. Chen, J.H. Li, M.F. Ge, Environ. Sci. Technol. 44 (2010) 9590–9596.
[19] Y.G. Ji, Z. Zhao, A.J. Duan, G.Y. Jiang, J. Liu, J. Phys. Chem. C 113 (2009) 7186–7199.
[20] I. Ayub, F.J. Berry, E. Crabb, O. Helgason, J. Mater. Sci. 39 (2004) 6921–6927.
[21] E. Park, O. Ostrovski, Isij Int. 44 (2004) 999–1005.
[22] M. Casapu, O. Krocher, M. Elsener, Appl. Catal. B-Environ. 88 (2009) 413–419.
[23] W.S. Kijlstra, M. Biervliet, E.K. Poels, A. Bliek, Appl. Catal. B-Environ. 16 (1998) 327–337.
[24] H.H. Phil, M.P. Reddy, P.A. Kumar, L.K. Ju, J.S. Hyo, Appl. Catal. B-Environ. 78 (2008) 301–308.
[25] J. Yu, F. Guo, Y.L. Wang, J.H. Zhu, Y.Y. Liu, F.B. Su, S.Q. Gao, G.W. Xu, Appl. Catal. B-Environ. 95 (2010) 160–168.
[26] G.S. Qi, R.T. Yang, J. Phys. Chem. B 108 (2004) 15738–15747.
[27] K.I. Hadjiivanov, Catal. Rev. 42 (2000) 71–144.
[28] W.S. Kijlstra, D.S. Brands, H.I. Smit, E.K. Poels, A. Bliek, J. Catal. 171 (1997) 219–230.
[29] S. Yang, C. Wang, J. Li, N. Yan, L. Ma, H. Chang, Appl. Catal. B-Environ. 110 (2011) 71–80.
[30] G. Busca, L. Lietti, G. Ramis, F. Berti, Appl. Catal. B-Environ. 18 (1998) 1–36.